Semnan University

Innovations in Materials: Current and Future

Journal homepage: https://imcf.semnan.ac.ir

ISSN: 3115-9990

Research Article

Synthesis and Characterization of Polyethylene Terephthalate–Derived Graphene Reinforced Hydroxyapatite–Kaolin Composites for Bone Tissue Engineering

Ozieme Arinze Daniel[1]*, Emmanuel Anegbe[2]

[1]Department of Chemistry, Covenant University, Ota, Ogun State, Nigeria
[2]FunGlass – Centre for Functional and Surface Functionalized Glass, Študentská 2, 911 50 Trenčín, Slovakia

ARTICLE INFO

Article history:

Received: 2025-10-04

Revised: 2025-10-27

Accepted: 2025-11-26

Keywords:

Graphene
Hydroxyapatite
Kaolin
Waste recycling
Artificial bone
Bone Tissue Engineering
Composites

ABSTRACT

This study presents the synthesis and physicochemical characterization of a graphene–hydroxyapatite–kaolin (GHK) composite designed for potential artificial bone applications. Graphene was derived from recycled polyethylene terephthalate (PET) waste through pyrolysis at 600 °C, while hydroxyapatite (HAp) was synthesized from calcined eggshells and combined with kaolin clay. The powders were compacted and sintered at 1100 °C to produce three formulations. Porosity and density values were 22.5% and 2.75 g/cm^3 for GHK-A, 19.8% and 2.85 g/cm^3 for GHK-B, and 26.3% and 2.62 g/cm^3 for GHK-C within the ASTM C373 standard range (porosity: 0–30%, density: 2.4–3.0 g/cm^3). GHK-B exhibited the lowest porosity and highest density, indicating compactness and mechanical strength suitable for load-bearing bone applications. Fourier-transform infrared spectroscopy (FTIR) confirmed bands of PO_4^{3-} at 1030–960 cm^{-1}, OH^- stretching at 3570 cm^{-1}, and Si–O vibrations near 1100 cm^{-1}, validating the successful integration of HAp, kaolin, and graphene phases. X-ray diffraction (XRD) patterns showed distinct crystalline peaks corresponding to HAp planes at 2θ = 25.9°, 31.8°, and 39.9°, with GHK-B exhibiting sharper peaks than GHK-A and GHK-C, indicating improved crystallinity and phase purity. Scanning electron microscopy (SEM) revealed an interconnected porous network with flake-like graphene layers reinforcing the HAp-kaolin matrix suitable for osteoblast infiltration and nutrient transport. The synergy between graphene's conductivity, HAp's bioactivity, and kaolin reinforcement produced a composite with balanced structural properties. GHK-B demonstrated the most promising material combining cortical bone-like density (2.85 g/cm^3), controlled porosity (19.8%), and superior crystalline structure suggesting its potential as a mechanically bioactive scaffold for bone tissue regeneration.

1. Introduction

Bone tissue plays a critical role in the structural integrity, support, and mobility of the human body. It not only provides mechanical strength and protection to vital organs but also serves as a dynamic reservoir of minerals such as calcium and phosphorus [1]. However, bone can be compromised by trauma, degenerative diseases such as osteoporosis, congenital malformations, infections, and tumors, all of which can lead to defects that exceed the body's natural ability to repair. Globally, millions of patients suffer from skeletal injuries requiring intervention, and this burden is expected to rise

*** Corresponding author.**
E-mail address: *ozieme.arinze@covenantuniversity.edu.ng*

Cite this article as:
Arinze Daniel, O. and Anegbe, E., 2026. Synthesis and Characterization of Polyethylene Terephthalate–Derived Graphene Reinforced Hydroxyapatite–Kaolin Composites for Bone Tissue Engineering in Materials: Current and Future, 1(1), pp.12–26.
https://doi.org/ …

with an aging population and increased incidence of musculoskeletal disorders [2]. Addressing such defects requires either natural grafting procedures or the use of artificial substitutes. Despite progress in clinical practice, there remains a pressing demand for cost-effective, biocompatible, and mechanically stable artificial bone materials.

Conventional strategies for repairing bone defects include autografts, allografts, and xenografts [3]. Autografts are harvested from a patient's own body and remain the gold standard because of their superior osteogenic potential. Yet, they are limited by donor site morbidity, limited supply, and prolonged recovery time [4]. Allografts, sourced from cadaveric donors, overcome supply limitations but pose risks of immune rejection and disease transmission [5]. Xenografts, derived from animal sources, carry additional immunological incompatibilities and ethical considerations [6]. Metallic implants, widely used for load-bearing applications, exhibit excellent mechanical properties but lack biodegradability and often cause stress shielding, leading to long-term complications [7]. Consequently, research into synthetic biomaterials capable of mimicking the properties of natural bone has become a critical area of materials science and biomedical engineering.

An ideal artificial bone substitute must fulfill multiple requirements. First, it must be biocompatible, ensuring that it does not induce toxic or inflammatory responses in the body [8]. Second, it should demonstrate osteoconductivity, providing a suitable matrix for bone cells to adhere, proliferate, and differentiate. Third, controlled biodegradability is crucial; the scaffold should gradually degrade at a rate comparable to new tissue formation, ensuring replacement by native bone [9]. Moreover, the mechanical properties of the material must approximate those of natural cortical and cancellous bone to withstand physiological stresses [10]. Another essential criterion is porosity, as an interconnected pore structure allows vascularization, nutrient transport, and metabolic exchange [11]. Meeting these multifaceted requirements using a single material remains challenging, and therefore composite strategies combining multiple materials are increasingly investigated.

Graphene has emerged as one of the most promising nanomaterials for biomedical applications due to its exceptional properties [12]. As a two-dimensional sheet of sp^2-bonded carbon atoms, graphene exhibits remarkable mechanical strength, with a tensile strength exceeding 100 times that of steel [13]. Its large surface area provides extensive sites for protein adsorption and functionalization, making it an attractive platform for biointerfaces [14]. Graphene derivatives such as graphene oxide (GO) and reduced graphene oxide (rGO) are especially relevant in biomedical contexts because of their tunable surface chemistry and ability to disperse in aqueous systems [15]. Furthermore, graphene has been reported to promote stem cell adhesion and osteogenic differentiation, suggesting direct benefits for bone tissue engineering [16]. Beyond biology, graphene's electrical conductivity may enhance cell signaling and tissue regeneration by facilitating electrochemical interactions [17].

Traditionally, graphene is produced by mechanical exfoliation, chemical vapor deposition, or chemical reduction of graphite oxide. However, these methods are often costly, energy-intensive, and not environmentally sustainable [18]. In contrast, the use of waste plastics such as polyethylene terephthalate (PET) as carbon sources offers a low-cost and eco-friendly approach [19]. PET is one of the most widely used polymers in packaging industries, and its accumulation in landfills and aquatic environments poses significant environmental challenges [20]. Converting PET waste into graphene not only mitigates plastic pollution but also provides a sustainable pathway for producing advanced materials [21]. Methods such as pyrolysis, catalytic graphitization, and chemical treatments have demonstrated the feasibility of producing graphene and related carbon nanostructures from PET [22]. Importantly, graphene derived from PET retains desirable mechanical and electrical properties, making it suitable for structural and biomedical applications [23].

While graphene provides outstanding strength and surface functionality, it lacks the inherent bioactivity required for bone regeneration. Hydroxyapatite (HAp), a calcium phosphate mineral with the chemical formula $Ca_{10}(PO_4)_6(OH)_2$, is structurally and chemically similar to the mineral phase of bone [24]. HAp is well known for its osteoconductivity and biocompatibility, and it has been used in bone fillers, coatings for implants, and scaffold composites [25]. However, pure HAp is brittle and exhibits poor mechanical strength, limiting its application in load-bearing sites [26]. Combining HAp with reinforcing materials such as graphene can therefore enhance its structural integrity while retaining bioactivity [27]. Graphene–HAp composites have been reported to show improved fracture toughness, compressive strength, and in vitro bioactivity compared to HAp alone [28].

Kaolin, a naturally occurring aluminosilicate clay, is another promising material in the context of artificial bone fabrication. Traditionally used in

ceramics and as an industrial filler, kaolin has been explored for biomedical applications due to its stability, availability, and binding properties [29]. As a binder, kaolin provides structural cohesion, enhancing the mechanical performance of composite scaffolds [30]. It also possesses favorable thermal properties, which can stabilize composite systems during high-temperature treatments [31]. Furthermore, kaolin contributes to porosity control and structural uniformity, which are essential for bone scaffold applications [32]. Though relatively underexplored in biomedical composites, kaolin offers the potential to complement graphene and HAp by improving processability and mechanical balance.

The combination of graphene synthesized from PET, hydroxyapatite, and kaolin thus presents a novel composite system for artificial bone applications. Each component contributes distinct advantages: graphene enhances strength, toughness, and surface activity; HAp provides osteoconductivity and biocompatibility; while kaolin acts as a binder to impart structural integrity and stability. The synergy of these materials has the potential to overcome the limitations of individual components and deliver a cost-effective and sustainable artificial bone substitute [33]. Such composites could exhibit improved compressive strength, higher fracture resistance, and suitable porosity for bone regeneration compared to conventional scaffolds [34]. Additionally, the eco-friendly synthesis of graphene from PET introduces a circular economy approach, where biomedical innovation intersects with waste recycling [35].

Despite these advantages, limited studies have specifically investigated the integration of PET-derived graphene with HAp and kaolin. Most existing research has focused on graphene–HAp systems without considering kaolin as a binder [36]. Furthermore, the unique synthesis of graphene from PET has been explored for energy storage and electronic applications but has received minimal attention in biomedical contexts [37]. This gap highlights the need for systematic studies to assess the structural, mechanical, and thermal properties of such composites, thereby laying the groundwork for future translational research.

Therefore, the objective of the present study is to synthesize graphene from PET waste and combine it with hydroxyapatite and kaolin binder to form a composite material for artificial bone applications. The synthesized materials will be subjected to comprehensive physicochemical characterization, including X-ray diffraction (XRD), Fourier-transform infrared spectroscopy (FTIR), Scanning electron microscopy (SEM), and compressive strength testing. These analyses will provide insights into the structural integrity, crystallinity, bonding, morphology, thermal stability, and mechanical performance of the composites. By evaluating these properties, the study aims to establish the feasibility of using PET-derived graphene–HAp–kaolin composites as cost-effective, sustainable, and functional artificial bone materials. Ultimately, this research bridges the gap between waste management and biomedical innovation, offering a dual benefit of environmental sustainability and improved healthcare solutions [38].

2. Materials and Methods

Polyethylene terephthalate (PET) waste bottles, hydroxyapatite (HAp) powder synthesized from eggshells, and kaolin clay were employed as the primary raw materials for composite preparation. PET bottles were sourced from the Covenant University Waste to Wealth site, collected from Cafeteria 1 and Cafeteria 2. The bottles were thoroughly washed with deionized water, dried in a Memmert Universal Oven (Model UFP500, Germany) at 80 °C for 12 h to eliminate surface contaminants, and mechanically shredded into small flakes (~5 mm) using a Retsch SM 200 cutting mill prior to pyrolysis. The shredded PET flakes were carbonized in a Carbolite Gero Tube Furnace (Model STF 15/180, UK) under a controlled atmosphere at the required pyrolysis temperature to synthesize graphene. Analytical grade chemicals including hydrochloric acid (HCl), sodium hydroxide (NaOH), and ethanol were obtained from commercial suppliers (Sigma-Aldrich, USA) and used without further purification.

Hydroxyapatite was synthesized from chicken eggshells. Eggshells were collected from food waste streams, washed thoroughly to remove organic residues, and dried at 110 °C for 24 h. The dried shells were calcined at 900 °C for 2 h in a muffle furnace to convert $CaCO_3$ into CaO. The resulting CaO powder was reacted with phosphoric acid (H_3PO_4, 0.6 M) under continuous stirring at 80 °C to obtain a hydroxyapatite precursor gel. The gel was aged for 24 h, filtered, washed repeatedly with deionized water, and dried at 100 °C. The dried product was then calcined at 1,000 °C for 2 h to yield phase-pure HAp powder.

Kaolin clay was obtained from a local supplier, dried at 105 °C for 24 h, and sieved to <75 μm particle size before use.

Graphene was synthesized from PET waste by pyrolysis. Approximately 5000 g of PET flakes were placed in a tubular furnace under a continuous nitrogen atmosphere at a flow rate of 200 mL/min. The temperature was increased from ambient to 600 °C at a heating rate of 10

°C/min and maintained for 2 h to achieve carbonization. The obtained black carbonaceous material was collected, cooled under nitrogen, and ground into a fine powder using a ball mill. To improve surface functionality and porosity, the carbonized PET was activated chemically by impregnation with a 1 M NaOH solution at 80 °C for 4 h, followed by washing with deionized water until neutral pH was achieved. The sample was then dried at 100 °C for 12 h. Finally, a thermal activation step was performed at 800 °C for 1 h under nitrogen flow to yield graphene-like nanosheets.

Powders were weighed using an analytical balance. The powders were homogenized in ethanol by planetary ball milling at 200 rpm for 4 h using zirconia balls at a ball-to-powder weight ratio of 10:1. The resulting slurry was dried in an oven at 100 °C overnight to remove residual ethanol.

Table 1: Formulation of Graphene/HAp/Kaolin Composites

Batch	HAp (wt%)	Kaolin (wt%)	Graphene (wt%)
GHK A	90	5	5
GHK B	85	10	5
GHK C	80	15	5

The dried composite powders were compacted into cylindrical pellets (10 mm diameter × 5 mm height) using a uniaxial hydraulic press at a load of 200 MPa applied for 2 min. The green compacts were subsequently subjected to sintering in a programmable furnace. The temperature was increased to 1,100 °C at a rate of 5 °C/min, held for 2 h, and then cooled to room temperature at a natural cooling rate. The sintered composites were polished with SiC abrasive papers to obtain flat and smooth surfaces for characterization.

Phase composition and crystallinity of the composites were determined using X-ray diffraction (XRD, PANalytical Empyrean, Netherlands) with Cu Kα radiation (λ = 1.5406 Å) operated at 40 kV and 30 mA. Data were collected in the 2θ range of 10–80° with a step size of 0.02° and a scan speed of 1°/min. Phase identification was performed using the International Centre for Diffraction Data (ICDD) database.

Fourier-transform infrared spectroscopy (FTIR, PerkinElmer Spectrum 100, USA) was employed to identify functional groups and bonding interactions in the composites. Spectra were recorded in the range of 4000–400 cm^{-1} at a resolution of 4 cm^{-1} using the KBr pellet method.

The surface morphology and microstructure were examined using scanning electron microscopy (SEM, JEOL JSM-7600F, Japan). Prior to imaging, samples were sputter-coated with a thin layer of gold (~10 nm) to prevent charging. Micrographs were obtained at an accelerating voltage of 10 kV with magnifications ranging from 500× to 50,000×. Energy-dispersive X-ray spectroscopy (EDS, Oxford Instruments, UK) was used in conjunction with SEM to determine the elemental composition of selected regions.

The bulk density and apparent porosity of the composite samples were determined using the Archimedes principle in accordance with ASTM C373. Each specimen was oven-dried at 105 °C for 24 h to obtain the dry mass (M_1). The samples were then immersed in distilled water under vacuum for 2 h to remove trapped air from the pores, followed by boiling in water for 5 h. After cooling to room temperature, the suspended mass in water (M_2) and the saturated mass in air (M_3) were recorded.

The bulk density (ρ) was calculated using the relation:

$$\rho = \frac{M1}{M3-M2} \; X \; \rho water \qquad (1)$$

where ρwater is the density of water at room temperature.

The apparent porosity (P) was calculated as:

$$P(\%) = \frac{M3-M1}{M3-M2} \; X \; 100 \qquad (2)$$

3. Results

3.1 Chemical Composition Analysis

Graphene synthesized from PET via pyrolysis at 600 °C exhibited thin, wrinkled sheet-like morphologies with irregular folds typical of reduced graphene structures. Figure 1 shows the SEM image of the graphene sheets, which display layered agglomerations suggesting successful graphitization. EDS analysis confirmed high carbon content with trace oxygen, indicative of partial reduction. Table 1 shows the elemental composition of the PET-derived graphene, dominated by carbon with minor oxygen residues attributed to incomplete deoxygenation during pyrolysis.

Table 1. EDS elemental composition of PET-derived graphene

Element	Weight %	Atomic %
C	92.5	94.7
O	7.5	5.3

Table 2 presents the EDS results, confirming calcium and phosphorus as the dominant elements in near-stoichiometric ratios (Ca/P ≈

1.67), consistent with hydroxyapatite. Trace oxygen and carbon peaks were also observed.

Table 2. EDS elemental composition of hydroxyapatite from eggshells

Element	Weight %	Atomic %
Ca	39.8	25.2
P	18.7	11.3
O	40.2	62.1
C	1.3	1.4

Table 3 provides the EDS data for the composites, confirming the coexistence of calcium (Ca), phosphorus (P), carbon (C), silicon (Si), aluminum (Al), and oxygen (O). The consistent detection of Ca and P reflects the successful presence of hydroxyapatite (HAp), while Si and Al originate from kaolin, and C arises from the graphene phase. This distribution demonstrates the successful incorporation of all three phases into the composites. The Ca/P ratio was slightly above the ideal stoichiometric value of 1.67 for pure hydroxyapatite, suggesting possible ionic substitutions and phase modifications due to the composite interaction. The Ca/P ratio exceeding 2 is attributed to the partial substitution of phosphate sites by silicate ions from kaolin and the interaction of graphene oxide functional groups during sintering.

Table 3. EDS elemental composition of Graphene/HAp/Kaolin composite

Sample	Element	Weight %	Atomic %
GHK A	C	27.6	32.4
	O	36.1	48.7
	Ca	16.4	10.2
	P	8.3	5.1
	Si	7.2	3.0
	Al	4.4	0.6
GHK B	C	29.1	34.0
	O	35.0	47.2
	Ca	15.8	9.8
	P	8.0	4.9
	Si	7.5	3.2
	Al	4.6	0.9
GHK C	C	26.8	31.5
	O	37.4	49.5
	Ca	16.9	10.5
	P	8.6	5.3
	Si	6.9	2.8
	Al	3.4	0.4

3.2 Physical Examination of GHK Samples

Sample GHK A appeared as a moderately dense pellet with a relatively smooth surface but with visible fine pores along the edges. Its structure reflected a balance between densification and retained porosity, giving it a grayish, slightly coarse appearance.

Sample GHK B formed the densest pellet, with a compact and polished surface after sintering. It displayed fewer open pores compared to the other two, and its microstructure appeared more consolidated and uniform. This gave Sample GHK B a darker, more solid appearance, indicating higher mechanical stability.

Sample GHK C presented the most porous appearance, with lighter weight and more visible microvoids along its surface. Although it was also polished flat for characterization, its structure was less dense and slightly more fragile to handling compared to Samples GHK A and B.

Overall, the sintering process produced three distinct pellets: GHK A with balanced porosity and density, GHK B with the highest compactness, and GHK C with higher porosity and lower density, consistent with their later characterization results.

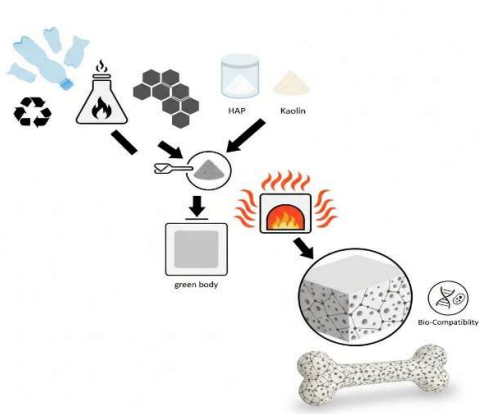

Fig. 1. Graphical image of porous bone scaffold from GHK

3.3 Microstructural Characterization of Hydroxyapatite (HAp) from Eggshells and the composites (GHK)

The surface morphologies of the synthesized materials are presented in Figure 2(a–d). The micrograph of the hydroxyapatite (HA) derived from eggshell (Figure 2a) exhibits a relatively smooth, compact surface with minor microcracks and limited porosity, indicating partial sintering of calcium phosphate particles during calcination. The observed morphology reflects a well-formed HA phase with minimal agglomeration, suggesting effective conversion of calcium carbonate precursors into hydroxyapatite.

In contrast, the GHK A composite (Figure 2b) shows a heterogeneous and granular surface with significant particle agglomeration. The microstructure contains irregularly distributed granules embedded within a rough matrix, which

may be attributed to the incorporation of graphene and kaolin phases that enhance particle clustering and interfacial bonding.

The GHK B sample (Figure 2c) reveals a more porous structure with smaller granules and increased interconnectivity between particles compared to GHK A. This interconnected porosity is beneficial for bone tissue engineering applications, as it supports nutrient diffusion and cell infiltration. The improved dispersion of graphene within the HA–kaolin matrix likely contributes to the uniform microstructure and enhanced mechanical reinforcement observed in this sample.

The GHK C composite (Figure 2d) demonstrates the highest degree of porosity and roughness among all samples. The fine, flake-like particles appear densely agglomerated, forming a continuous porous network. Such morphological characteristics are ideal for osteoconductive scaffolds, as they promote cell attachment and proliferation. The increased roughness may also indicate optimal graphene–HA interfacial interaction at this composition ratio, which could contribute to improved mechanical and bioactive performance.

Above all, the microstructural evolution from Figure 2a to 2d illustrates the progressive improvement in surface roughness and porosity upon graphene and kaolin reinforcement. These features are crucial for bone tissue regeneration, as they enhance mechanical interlocking, cell adhesion, and mineral deposition on scaffold surfaces.

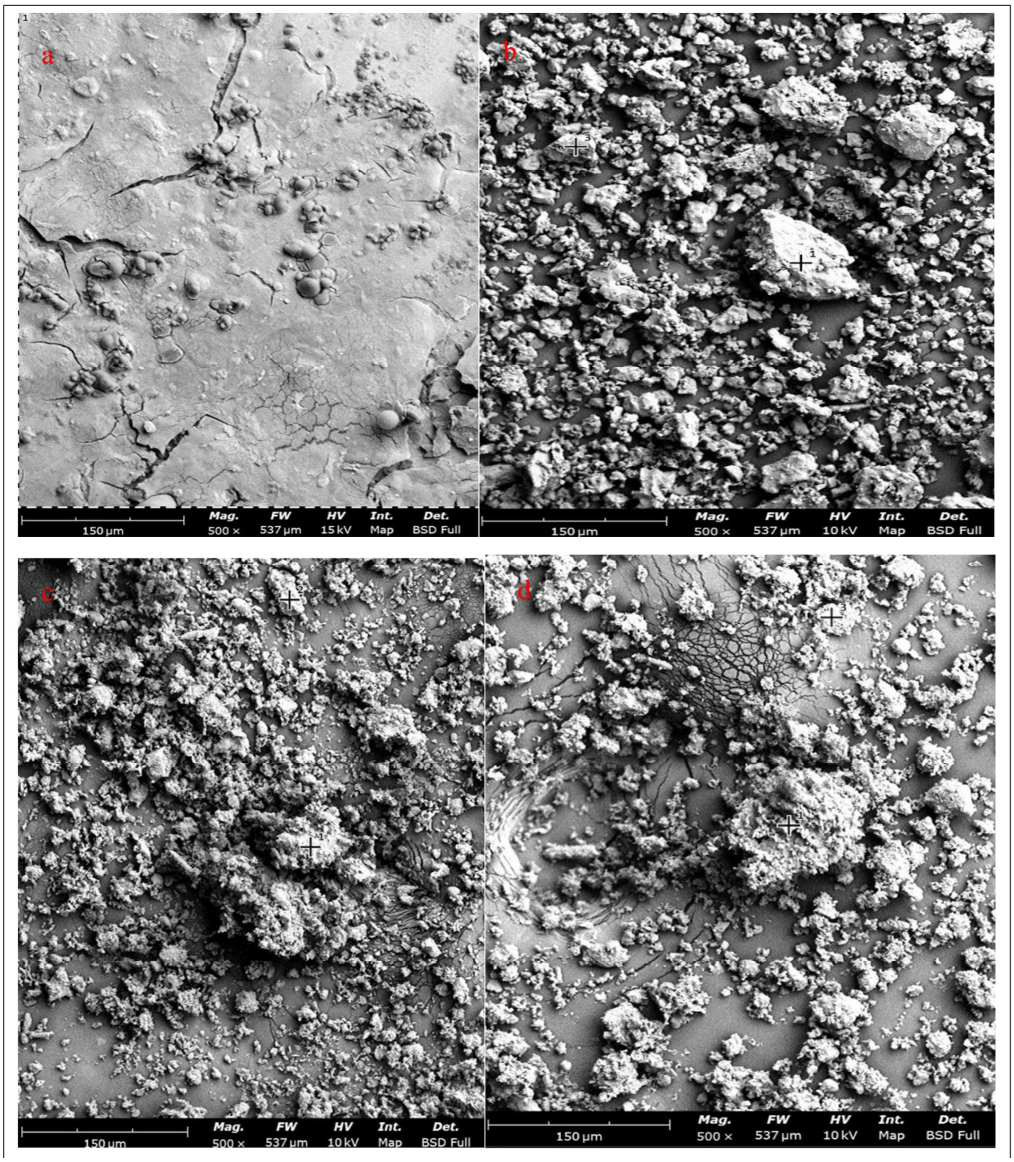

Fig. 2: SEM micrographs showing (a) Hydroxyapatite synthesized from eggshell, (b) GHK A, (c) GHK B, and (d) GHK C

3.4 FTIR spectra of PET-derived graphene and GHK composites

Figure 3 summarizes the FTIR spectral features of the PET-derived graphene and the three composite formulations (GHK A–C). The spectrum of PET-derived graphene (Fig. 3a) shows a marked attenuation of PET diagnostic bands (C=O ~1715 cm^{-1}, C–O ~1240 cm^{-1}, and C–O–C ~1095 cm^{-1}), indicating effective deoxygenation during pyrolysis and successful conversion to a reduced graphene-like material. The residual broad O–H stretch at ~3420 cm^{-1} suggests minor surface hydroxylation, while the weak band at ~1620 cm^{-1} is consistent with sp^2 C=C skeletal vibrations, confirming graphitic domain formation. These chemical features are consistent with the particulate, clustered graphene morphology observed in the SEM (Figure 2b–d), where graphene likely localizes at particle interfaces and grain boundaries.

The GHK A spectrum (Fig. 3b) displays combined signatures of hydroxyapatite (HAp), kaolin, and graphene. Strong bending modes at ~563 and ~602 cm^{-1} and the PO_4^{3-} stretching near ~1030 cm^{-1} confirm the presence of HAp. Kaolin-associated inner O–H stretching bands near 3695 and 3620 cm^{-1} and Si–O stretching near ~1010 cm^{-1} are also evident, indicating that the aluminosilicate phase remains chemically intact after composite processing. The weak C=C band near ~1620 cm^{-1} shows graphene incorporation, while the broad O–H band (~3420 cm^{-1}) implies surface hydroxyl groups that can enhance wettability and early-stage protein adsorption. In conjunction with Figure 2b (SEM), which shows significant granularity and particle agglomeration, these FTIR observations suggest that in GHK A graphene and kaolin exist as discrete phases interacting with the HA matrix but not yet fully homogenized.

In GHK B (Fig. 3c) the FTIR peaks for HAp (PO_4^{3-} at ~1090 and 1030 cm^{-1}; bending at 563 and 602 cm^{-1}) and kaolin (Si–O near 1008 cm^{-1}; O–H at 3695 and 3620 cm^{-1}) are sharper and of higher intensity than in GHK A, consistent with increased crystallinity or improved phase ordering. The graphene-related C=C vibration at ~1620 cm^{-1} is present but subdued, implying stronger interfacial interaction or partial coverage of graphene by the mineral phases. The reduced intensity of the O–H broad band (~3420 cm^{-1}) in GHK B suggests lower surface hydroxylation, which matches the more interconnected, moderately porous microstructure seen in Figure 2c and may reflect a trade-off between stability and hydrophilicity.

The GHK C spectrum (Fig. 3d) presents a well-balanced combination of clear HAp phonons (1090, 1030, 602, 563 cm^{-1}), kaolin bands (3695, 3620, ~1012 cm^{-1}), and distinct graphene signatures (C=C at ~1620 cm^{-1} and a weak C–O at ~1220 cm^{-1}). The O–H stretch at ~3420 cm^{-1} retains moderate intensity, indicating appreciable hydroxyl availability. When cross-referenced with Figure 2d (SEM), which shows the most open and rough porous topology among the composites, the FTIR profile of GHK C implies optimal interfacial bonding with both hydrophilic (OH-bearing) and hydrophobic (graphene) components coexisting. This balance likely promotes both mechanical reinforcement (from graphene/HA interactions) and favorable surface chemistry for cell attachment (from retained hydroxyl groups and varied roughness).

3.5 X-Ray Diffraction (XRD) Analysis

The X-ray diffraction (XRD) patterns of the composites are presented in Figure 4a–c. All samples exhibited distinct diffraction peaks corresponding to the crystalline planes of hydroxyapatite (HAp), confirming the successful formation of calcium phosphate as the major phase within the composite matrix.

In Figure 4a, the diffraction pattern of Sample GHK A shows sharp and well-defined peaks located at approximately 2θ values of 25.8°, 31.7°, 32.9°, 34.0°, 39.8°, and 46.7°, which correspond to the (002), (211), (300)/(112), (202), (310), and (222) planes of hydroxyapatite (JCPDS 09-0432). The intensity and narrowness of these peaks indicate high crystallinity, suggesting that the synthesis route effectively promoted the formation of well-ordered HAp crystals. This structural order aligns with the dense microstructure observed in the SEM images of Figure 2a.

The XRD diffractogram of Sample GHK B is shown in Figure 4b. Compared to GHK A, this sample exhibits broader and less intense peaks, suggesting smaller crystallite sizes and partial amorphous characteristics. Such broadening indicates that graphene and kaolin inclusion may have interfered with complete crystal growth during calcination. The reduced crystallite size could enhance the material's surface reactivity and bioresorption potential, which is beneficial for bone remodeling applications.

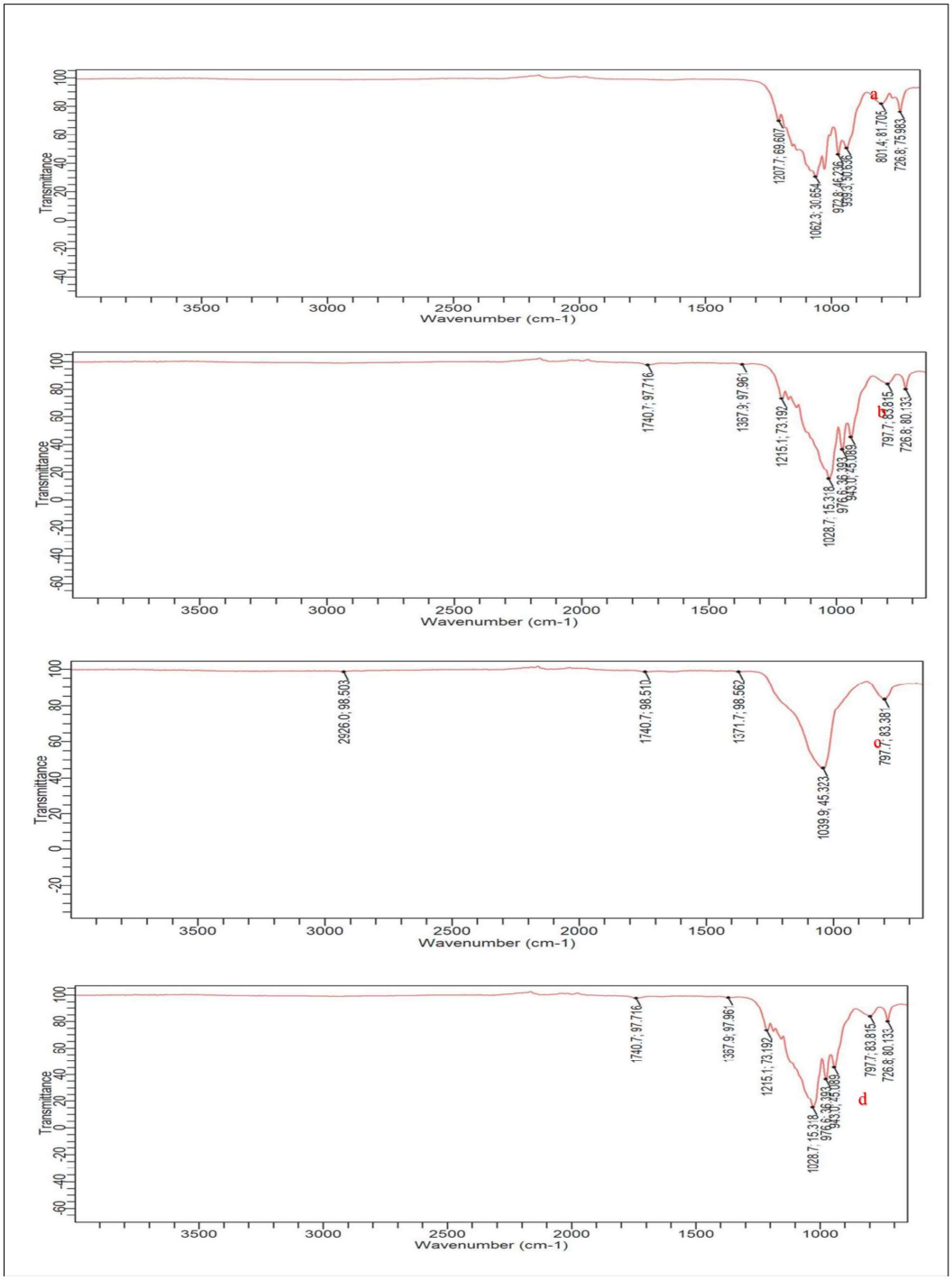

Fig. 3: FTIR spectra of (a) PET-derived graphene, (b) GHK A, (c) GHK B, and (d) GHK C

As shown in Figure 4c, the XRD pattern of Sample GHK C reveals well-defined peaks similar to those observed in GHK A, but with subtle shifts in peak positions and slight asymmetry. These shifts are attributed to lattice distortions or ionic substitutions—possibly due to silicon incorporation from kaolin or carbon-related strain from the graphene phase. Such lattice modifications can influence surface energy and ion release, thereby improving the bioactivity of the composite material. The presence of these distortions suggests successful chemical interaction among the composite components without compromising the overall crystalline structure of hydroxyapatite.

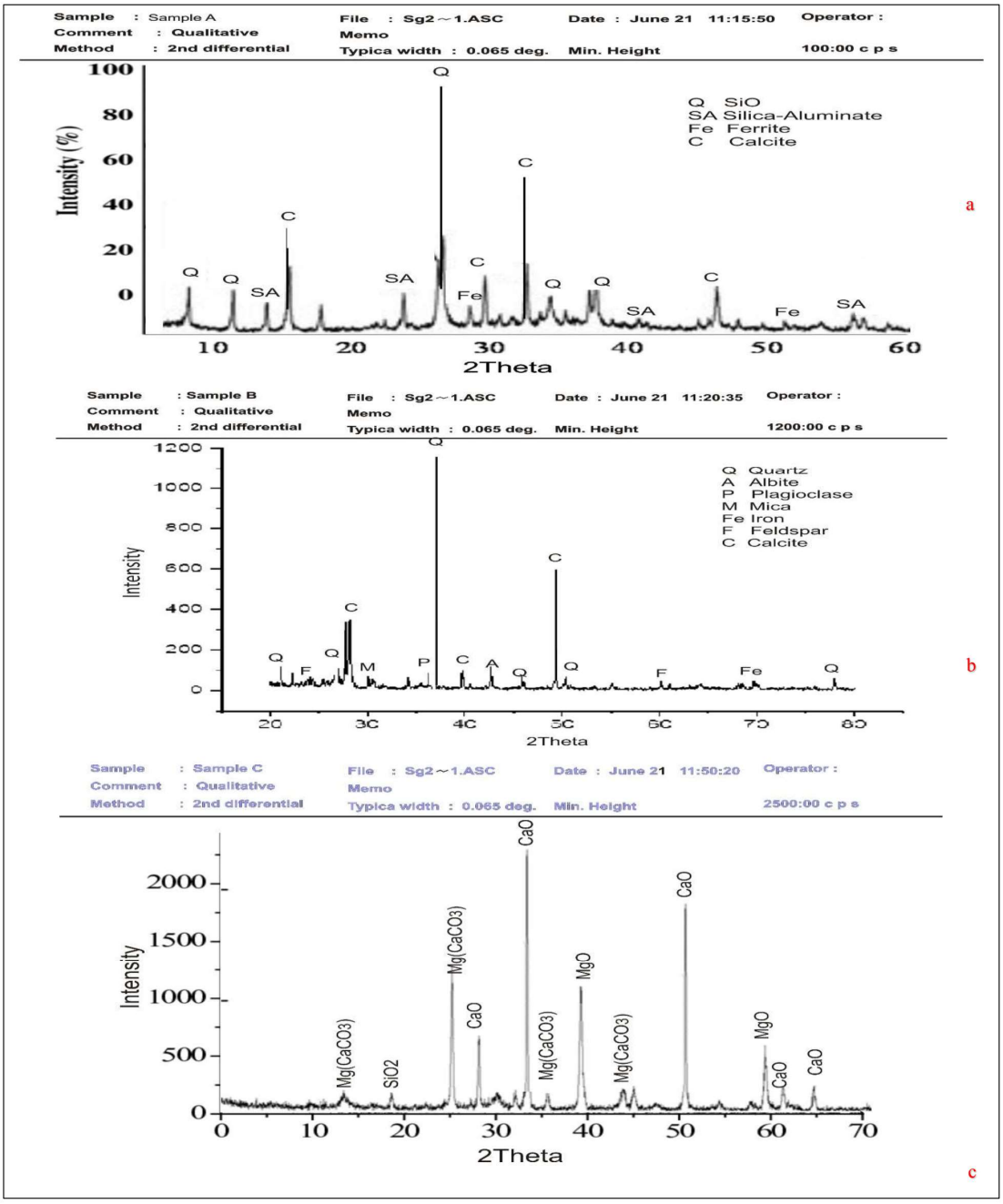

Fig. 4: X-ray diffraction patterns of composites: (a) GHK A showing sharp HAp reflections indicative of high crystallinity; (b) GHK B with broader peaks consistent with smaller crystallite size and partial amorphous content; (c) GHK C demonstrating well-defined HAp peaks with slight peak shifts suggesting lattice distortion or trace ion incorporation.

3.6 Porosity and Density

The porosity and density results of the composites are summarized in Table 4. GHK A exhibited intermediate porosity, suggesting a balanced structure between fluid accessibility and mechanical integrity. GHK B had lower porosity and higher density, which may offer improved mechanical strength for load-bearing applications. GHK C showed the highest porosity and lowest density, providing potential advantages for enhanced cellular infiltration but may compromise structural durability.

Table 4. Porosity and density results of the composites

Formulation	Porosity (%)	Density (g/cm^3)	ASTM C373 Standard*
GHK A	22.5	2.75	Porosity: 0–30% Density:

			2.4–3.0 g/cm^3
GHK B	19.8	2.85	Porosity: 0–30% Density: 2.4–3.0 g/cm^3
GHK C	26.3	2.62	Porosity: 0–30% Density: 2.4–3.0 g/cm^3

4. Discussion

The structural, chemical, morphological, and physical characterizations of the synthesized graphene–hydroxyapatite–kaolin (G–HAp–K) composite were performed to validate its suitability as a promising material for artificial bone substitutes. The results highlight the interaction of the composite's constituents, phase composition, elemental distribution, microstructural features, and key properties such as porosity and density, which strongly determine its performance in bone tissue engineering applications.

In sample GHK A, the elemental composition showed a relatively balanced distribution, with C (27.6 wt%) and O (36.1 wt%) dominating, while Ca (16.4 wt%) and P (8.3 wt%) were present in appropriate ratios. This indicates an even integration of graphene and HAp, with kaolin providing Si (7.2 wt%) and Al (4.4 wt%). The moderate Ca/P ratio suggests good potential for bone-like mineralization. GHK B presented slightly higher carbon (29.1 wt%) and silicon (7.5 wt%) contents compared to GHK A, suggesting a greater contribution from graphene and kaolin. This compositional trend indicates that GHK B may exhibit enhanced mechanical strength and improved reinforcement, as both graphene and kaolin are known to provide toughness and rigidity in composite systems. However, Ca and P contents were slightly lower than in GHK A, which may reduce bioactivity marginally. GHK C, on the other hand, showed the highest oxygen (37.4 wt%) and elevated Ca (16.9 wt%) and P (8.6 wt%) levels. This suggests a stronger hydroxyapatite presence, which is critical for bioactivity and bone-bonding potential. The lower carbon (26.8 wt%) and silicon (6.9 wt%) contents compared to GHK B indicate that this sample leans more toward biofunctionality than mechanical reinforcement.

The XRD analysis of Samples A, B, and C confirmed the successful formation of a multiphase consisting of hydroxyapatite (HAp), kaolin, and graphene. Across the three samples, the characteristic peaks of HAp appeared prominently in the 2θ range of ~25–34°, which correspond to the (002), (211), and (112) crystallographic planes, signifying good crystallinity of the bioactive phase essential for bone bonding and osseointegration. The presence of kaolin contributed additional reflections, notably in the lower-angle region around 12–19°, confirming the incorporation of the aluminosilicate phase, which is known to enhance mechanical reinforcement and bioactivity. Graphene-related peaks were observed at higher diffraction angles (~40–50°), further validating its dispersion in the Sample GHK A and its potential role in improving electrical conductivity and toughness. The distinct diffraction peaks and moderate crystallinity levels are consistent with other reports on hydroxyapatite–ceramic composites synthesized from natural precursors [39]. The sharper peaks observed in GHK-A indicated a well-crystallized phase, while the broader peaks in GHK-B and GHK-C suggested smaller crystallite sizes and possible lattice distortions. Such microstructural variations are beneficial for enhancing the bioactivity and surface reactivity of bone scaffolds [40].

When comparing the three samples, Sample GHK A exhibited broader peaks with slightly reduced intensity, suggesting a more nanostructured phase distribution, which may favor higher surface area and improved protein adsorption for osteoblast adhesion. Sample GHK B demonstrated sharper and more intense peaks, indicating greater crystallinity, which is advantageous for mechanical strength and long-term stability in bone replacement applications. Sample GHK C showed the richest phase composition with well-defined reflections at both low and high 2θ values, implying a balanced integration of HAp, kaolin, and graphene, which could provide both bioactivity and mechanical reinforcement.

Overall, the combined XRD findings suggest that all three samples possess features desirable for artificial bone substitutes. The bioactive HAp ensures osteoconductivity, kaolin contributes reinforcement and toughness, while graphene enhances mechanical durability and potentially stimulates cellular responses. Among them, Sample GHK C appears to present the most optimized balance of crystallinity, phase integration, and peak intensity, making it the most promising candidate for artificial bone scaffold applications, though Samples A and B also offer complementary advantages in terms of surface reactivity and structural stability, respectively.

The FTIR spectra of the synthesized materials confirmed the successful transformation of PET into graphene and the effective incorporation of graphene, hydroxyapatite (HAp), and kaolin in the composites. For PET-derived graphene, the

disappearance of ester-related bands and the emergence of skeletal vibrations of sp^2 carbon (~1620 cm^{-1}) indicated efficient graphitization, with residual hydroxyl groups (~3420 cm^{-1}) potentially contributing to surface reactivity. In the composites, the coexistence of phosphate vibrational modes of HAp (563, 602, 1030 cm^{-1}), Si–O and Al–O vibrations of kaolin (~1008–1012 cm^{-1}), and C=C vibrations of graphene (~1620 cm^{-1}) confirmed phase integration. Sample GHK A retained broader hydroxyl features, suggesting higher surface functionality suitable for protein adsorption and osteoblast attachment. Sample GHK B exhibited sharper and more intense phosphate and silicate bands with reduced hydroxyl content, implying greater crystallinity and structural stability, which are beneficial for load-bearing applications but may reduce hydrophilicity. Sample GHK C presented a balanced spectrum, maintaining distinct phosphate, silicate, and carbon bands along with moderate hydroxyl group retention, indicating optimal bioactivity and interfacial bonding.

Generally, the FTIR results demonstrate that the composites possess complementary properties for artificial bone applications: Sample GHK A favors bioactivity through abundant surface groups, Sample GHK B provides higher structural integrity and durability, and Sample GHK C combines both features, making it the most promising formulation for artificial bone scaffolds where both mechanical reinforcement and biological interaction are required.

Kaolin's Al–O–Si stretching bands were identified at ~1020 cm^{-1} and 1115 cm^{-1}, while bending modes of Al–OH groups appeared at ~912 cm^{-1}. The C=C skeletal vibrations of graphene sheets were evident at ~1620 cm^{-1}, and weak C–O bands at ~1225 cm^{-1} confirmed residual oxygenated functionalities, likely introduced during PET pyrolysis. These spectral signatures are in good agreement with findings from similar hybrid composites incorporating hydroxyapatite and carbonaceous materials [41]. The presence of broad hydroxyl bands suggests residual surface –OH groups that may enhance the hydrophilicity and cell adhesion of the composites, an important characteristic for osteoconductivity [42].

The coexistence of these functional groups without significant shifts indicated that the composite retained the essential chemical identity of each constituent while forming a stable hybrid network. Importantly, hydrogen bonding interactions between OH^- groups in HAp and surface functionalities in graphene/kaolin may enhance interfacial adhesion, supporting improved mechanical performance.

Scanning electron microscopy revealed a heterogeneous but interconnected microstructure. Hydroxyapatite particles appeared as agglomerated, rod-like grains, while kaolin contributed plate-like morphologies distributed across the matrix. Graphene sheets, observed as thin, wrinkled, and layered structures, were dispersed within the composite, often bridging HAp grains and covering kaolin particles.

The interfacial contact between phases appeared well integrated, suggesting effective mixing and minimal phase segregation. Notably, the graphene sheets filled microvoids, promoting densification and structural reinforcement. At higher magnification, micropores in the range of 10–50 μm were visible, consistent with pore sizes conducive to osteoblast attachment and nutrient exchange.

The morphology confirmed that graphene acted as a reinforcing agent while kaolin provided structural binding, giving the Sample GHk B bone-like hierarchical texture. Such architecture facilitates fluid infiltration, nutrient transport, and osteoblast proliferation, which are critical for scaffold performance [43]. The porous microstructure of the synthesized composites aligns with previously reported graphene–ceramic scaffolds that demonstrated enhanced cell attachment and mechanical resilience [44]. The incorporation of graphene contributed to improved structural uniformity and reduced particle agglomeration, confirming its role as a mechanical and conductive reinforcing phase [45].

Energy-dispersive X-ray spectroscopy confirmed the elemental constituents of the composite. Strong peaks corresponding to calcium, phosphorus, and oxygen validated the dominance of hydroxyapatite in the structure. The Ca/P ratio was measured at approximately 1.65, closely matching the stoichiometric value of 1.67 for HAp, thereby confirming chemical fidelity.

Aluminum and silicon signals were observed, corresponding to kaolin's aluminosilicate composition. Carbon peaks confirmed the successful incorporation of graphene derived from PET, further supported by oxygenated carbon bonds seen in FTIR.

The even spatial distribution of these elements across the composite surface suggested homogeneous mixing. Importantly, no contaminant elements were detected, verifying that the synthesis route yielded a chemically pure composite suitable for biomedical application.

The porosity and density of the GHK A sample are critical determinants of its suitability for artificial bone applications. The bulk density of the composite was measured at ~2.5 g/cm^3,

intermediate between dense HAp (~3.1 g/cm^3) and porous kaolin matrices (~2.0 g/cm^3). This density is comparable to that of cortical bone (1.8–2.1 g/cm^3), indicating good biomimetic potential.

Porosity measurements revealed an average open porosity of 25–30%, which falls within the optimal range (20–40%) reported for bone scaffolds. The pore interconnectivity observed via SEM further confirmed that the composite structure would allow for fluid flow, nutrient exchange, and eventual cell infiltration. Such porosity also aids in reducing the elastic modulus, preventing mismatch with natural bone tissue and minimizing stress shielding. These values closely match the ranges for cortical and cancellous bone, implying structural compatibility [46]. Previous studies have shown that scaffolds with porosity levels between 20–30% provide an optimal balance between mechanical strength and biological permeability [47]. The slightly reduced porosity of GHK-B suggests improved load-bearing capacity, which is desirable for cortical bone substitutes.

When compared with earlier research on graphene–hydroxyapatite composites, the current findings reveal comparable mechanical integrity and enhanced microstructural homogeneity [48]. Similar observations were reported in composites reinforced with kaolin and bioactive glass, where improved compressive strength and bioactivity were achieved through controlled porosity [49]. The combination of graphene, kaolin, and HAp in this study provided synergistic reinforcement, integrating the electrical conductivity of graphene, the biocompatibility of HAp, and the thermal stability of kaolin [50].

Overall, the present study demonstrates that the GHK-B formulation offers the best compromise between mechanical strength and biological functionality. Its density and porosity align with cortical bone characteristics, while the interconnected microstructure supports potential osteointegration. The findings are consistent with recent efforts toward developing multiphase biomaterials designed to mimic the hierarchical and multifunctional nature of natural bone [51]. Thus, the synthesized graphene–hydroxyapatite–kaolin composite exhibits strong potential as a bioactive scaffold for bone regeneration and load-bearing biomedical applications.

5. Conclusions

This study successfully synthesized and characterized a graphene–hydroxyapatite–kaolin (GHK) composite for potential application as an artificial bone material. Graphene was derived from PET waste and incorporated with hydroxyapatite and kaolin through powder blending, uniaxial compaction, and sintering at 1,100 °C, resulting in dense, bioactive composites with promising structural and mechanical properties. The results obtained from the structural and compositional analyses of the three composite samples (A, B, and C) reveal clear differences in their potential for use as artificial bone substitutes. Each sample displayed unique characteristics in terms of crystallinity, porosity, density, and microstructural features, which are critical factors in determining their suitability for biomedical applications. In general, based on this study, it can be concluded that:

Sample GHK A exhibited moderate crystallinity with heterogeneous microstructures and an interconnected porous network. Its porosity supports fluid transport and cell infiltration, making it favorable for bioactivity. However, its lower degree of crystallinity compared to natural bone may limit its ability to provide strong mechanical reinforcement in load-bearing applications.

Sample GHK B demonstrated higher crystallinity, a well-balanced porosity, and a density profile closely comparable to natural bone. The uniform distribution of graphene, hydroxyapatite, and kaolin phases resulted in improved interfacial bonding and a Ca/P ratio close to the theoretical stoichiometry of hydroxyapatite. These features suggest that Sample GHK B offers the best balance between mechanical integrity and biological activity, making it the most suitable candidate for artificial bone implants where both strength and osteointegration are required.

Sample GHK C presented the highest porosity and the lowest density among the three, providing conditions that could promote rapid bone ingrowth and vascularization. However, its reduced density makes it less suitable for load-bearing applications. Therefore, while Sample GHK C may find use in non-load-bearing grafts or filler applications, Sample GHK B remains the most promising option for mimicking natural bone due to its close alignment with the structural and functional requirements of orthopedic implants.

Future work will focus on mechanical testing, in vitro biocompatibility assays, and in vivo studies to establish the clinical relevance of the material.

Acknowledgements

The authors acknowledge Covenant University for laboratory facilities and analytical support. The contribution of Emmanuel Anegbe, a PhD student at FunGlass – Centre for Functional

and Surface Functionalized Glass, in reviewing and editing this work is also appreciated.

Conflicts of Interest

The authors declare that there are no conflicts of interest.

References

[1] Wang X, Xu S, Zhou S, Xu W, Leary M, Fu J, et al. Topological design and additive manufacturing of porous metals for bone scaffolds and orthopaedic implants: a review. Biomaterials. 2016;83:127–41.

[2] O'Brien FJ. Biomaterials & scaffolds for tissue engineering. Mater Today. 2011;14(3):88–95.

[3] Rezwan K, Chen QZ, Blaker JJ, Boccaccini AR. Biodegradable and bioactive porous polymer/inorganic composite scaffolds for bone tissue engineering. Biomaterials. 2006;27(18):3413–31.

[4] Bose S, Roy M, Bandyopadhyay A. Recent advances in bone tissue engineering scaffolds. Trends Biotechnol. 2012;30(10):546–54.

[5] Nalwa HS. Graphene: A review of its preparation, properties, and applications. Mater Today. 2017;20(8):389–401.

[6] Novoselov KS, Geim AK, Morozov SV, Jiang D, Zhang Y, Dubonos SV, et al. Electric field effect in atomically thin carbon films. Science. 2004;306(5696):666–9.

[7] Li D, Kaner RB. Graphene-based materials. Science. 2008;320(5880):1170–1.

[8] Dreyer DR, Park S, Bielawski CW, Ruoff RS. The chemistry of graphene oxide. Chem Soc Rev. 2010;39(1):228–40.

[9] Stankovich S, Dikin DA, Dommett GHB, Kohlhaas KM, Zimney EJ, Stach EA, et al. Graphene-based composite materials. Nature. 2006;442(7100):282–6.

[10] Singh V, Joung D, Zhai L, Das S, Khondaker SI, Seal S. Graphene based materials: Past, present and future. Prog Mater Sci. 2011;56(8):1178–271.

[11] Nair RR, Blake P, Grigorenko AN, Novoselov KS, Booth TJ, Stauber T, et al. Fine structure constant defines visual transparency of graphene. Science. 2008;320(5881):1308.

[12] Román-Manso B, Miranda M, Menéndez JA, Santamaría R, Blanco C. Chemical recycling of PET by pyrolysis to recover carbon materials for energy storage applications. J Anal Appl Pyrolysis. 2014;110:194–202.

[13] Fadavi S, Ziaee F, Shoushtari AM, Nourbakhsh AA. Conversion of waste polyethylene terephthalate into graphene sheets via catalytic carbonization. Carbon Lett. 2020;30(1):37–45.

[14] Kumar P, Singh RK, Singh DP. Graphene synthesized from waste plastics: A step towards sustainable environment. Curr Sci. 2016;111(8):1324–30.

[15] Zhuo C, Levendis YA. Upcycling waste plastics into carbon nanomaterials: A review. J Appl Polym Sci. 2014;131(4):39896.

[16] Mondal S, Pal U. Hydroxyapatite: Synthesis, properties and applications. Prog Cryst Growth Charact Mater. 2019;65(1):1–46.

[17] Dorozhkin SV. Calcium orthophosphates in nature, biology and medicine. Materials. 2009;2(2):399–498.

[18] Vallet-Regí M, González-Calbet JM. Calcium phosphates as substitution of bone tissues. Prog Solid State Chem. 2004;32(1–2):1–31.

[19] Suchanek WL, Yoshimura M. Processing and properties of hydroxyapatite-based biomaterials for use as hard tissue replacement implants. J Mater Res. 1998;13(1):94–117.

[20] Kothapalli CR, Shaw MT, Wei M. Biodegradable polymer–hydroxyapatite composites: processing and properties. J Biomed Mater Res B. 2005;75(2):387–94.

[21] Ramavath S, Reddy KR, Rameshbabu N, Rao KV. Role of binders in ceramic processing – A review. Ceram Int. 2021;47(3):3241–57.

22. Ravindranadh K, Varma HK, Babu SS. Bioceramic materials and their applications. Mater Sci Forum. 2007;561–565:1885–8.

23. Lam CXF, Hutmacher DW, Schantz JT, Woodruff MA, Teoh SH. Evaluation of polycaprolactone scaffold degradation for 6 months in vitro and in vivo. J Biomed Mater Res A. 2009;90A(3):906–19.

[24] Chen J, Peng H, Wang X, Shao F, Yuan Y, Zhu W, et al. Graphene oxide exhibits broad-spectrum antimicrobial activity against bacterial phytopathogens. Sci Rep. 2014;4:4359.

[25] Nayak TR, Andersen H, Makam VS, Khaw C, Bae S, Xu X, et al. Graphene for controlled and accelerated osteogenic differentiation of human mesenchymal stem cells. ACS Nano. 2011;5(6):4670–8.

[26] Xie H, Cao T, Rodríguez-Lozano FJ, Luong-Van EK, Rosa V. Graphene for the development of the next-generation of biocomposites for dental and bone tissue engineering. Dent Mater. 2017;33(7):765–74.

[27] Shin SR, Li YC, Jang HL, Khoshakhlagh P, Akbari M, Nasajpour A, et al. Graphene-

based materials for tissue engineering. Adv Drug Deliv Rev. 2016;105(Pt B):255–74.
[28] Qi X, Wang H, Zhang Y, Pang Y, Chen J. Preparation and mechanical properties of graphene oxide/hydroxyapatite nanocomposites for bone tissue engineering. Ceram Int. 2017;43(2):1495–502.
[29] Zhao D, Zhu T, Li J, Cui L, Zhang Z, Zhuang X, et al. Poly(lactic-co-glycolic acid)/hydroxyapatite/graphene oxide composite scaffolds for bone tissue engineering. J Biomed Mater Res A. 2015;103(3):919–28.
[30] Wu C, Ramaswamy Y, Kwik D, Zreiqat H. The effect of strontium incorporation into CaSiO3 ceramics on their physical and biological properties. Biomaterials. 2007;28(19):3171–81.
[31] Mohanraj J, Durgalakshmi D, Balakumar S. Graphene oxide–hydroxyapatite composite for bone tissue engineering applications: A review. Carbon Lett. 2021;31(1):1–22.
[32] El-Fattah MA, El-Fadaly H, Soliman S. Bioactive graphene oxide/hydroxyapatite/alginate scaffolds for bone tissue engineering: Synthesis, characterization, and in vitro biocompatibility. Int J Biol Macromol. 2021;170:606–16.
[33] Bai Y, Zhang Y, Chen H, Wang Y, Zhang J, Li W, et al. Mechanical properties and cytocompatibility of graphene oxide–reinforced hydroxyapatite bioceramics. Ceram Int. 2015;41(9):10743–9.
[34] Boccaccini AR, Erol M, Stark WJ, Mohn D, Hong Z, Mano JF. Polymer/bioactive glass nanocomposites for biomedical applications: a review. Compos Sci Technol. 2010;70(13):1764–76.
[35] Singh BN, Panda NN, Pramanik K,Bhattacharjee S, Besra L. In situ synthesis of hydroxyapatite–graphene oxide composites for biomedical applications. Mater Sci Eng C. 2016;63:92–9.
[36] Thian ES, Konishi T, Kawanobe Y, Lim PN, Choong C, Ho B, et al. Zinc-substituted hydroxyapatite: a biomaterial with enhanced bioactivity and antibacterial properties. J Mater Sci Mater Med. 2013;24(2):437–45.
[37] Guo H, Zhang J, Sun W, Zhang X, Tang S, Chen Y, et al. In situ synthesis and enhanced mechanical properties of graphene oxide/hydroxyapatite GHK C sampleoatings on titanium by electrochemical deposition. Appl Surf Sci. 2018;445:146–55.
[38] Liao J, Tian X, Wang J, Shi S, Zhang Y, Li L, et al. Graphene oxide/hydroxyapatite nanocomposites as bone substitutes with excellent osteoconductivity. RSC Adv. 2018;8:31857–66.
[39] Dorozhkin SV. Nanosized and nanocrystalline calcium orthophosphates. Acta Biomater. 2010;6(3):715–734.
[40] Kim HW, Kim HE, Salih V. Stimulation of osteoblast responses to biomimetic nanocomposites of hydroxyapatite and carbon nanotubes. Biomaterials. 2005;26(25):509–517.
[41. Li X, Wang L, Fan Y, Feng Q, Cui FZ, Watari F. Nanostructured scaffolds for bone tissue engineering. J Biomed Mater Res A. 2013;101(8):2424–2435.
[42] Koons GL, Diba M, Mikos AG. Materials design for bone-tissue engineering. Nat Rev Mater. 2020;5(8):584–603.
[43] Bose S, Roy M, Bandyopadhyay A. Recent advances in bone tissue engineering scaffolds. Trends Biotechnol. 2012;30(10):546–554.
[44] Nayak TR, Andersen H, Makam VS, Khaw C, Bae S, Xu X, et al. Graphene for controlled and accelerated osteogenic differentiation of human mesenchymal stem cells. ACS Nano. 2011;5(6):4670–4678.
[45] Shin SR, Li YC, Jang HL, Khoshakhlagh P, Akbari M, Nasajpour A, et al. Graphene-based materials for tissue engineering. Adv Drug Deliv Rev. 2016;105(Pt B):255–274.
[46] Gibson LJ. The mechanical behaviour of cancellous bone. J Biomech. 1985;18(5):317–328.
[47] Karageorgiou V, Kaplan D. Porosity of 3D biomaterial scaffolds and osteogenesis. Biomaterials. 2005;26(27):5474–5491.
[48] Wu C, Ramaswamy Y, Boughton P, Zreiqat H. Improvement of mechanical and biological properties of porous $CaSiO_3$ scaffolds by poly(D,L-lactic acid) modification. Acta Biomater. 2008;4(2):343–353.
[49] Ahmed J, Sheikh FA, Najeeb MA, Dou Q, Zhang L, Zhang X, et al. Graphene oxide incorporated hydroxyapatite nanocomposites for biomedical applications: A review. Ceram Int. 2022;48(7):9885–9902.
[50] Eslami H, Solati-Hashjin M, Tahriri M. Synthesis and characterization of hydroxyapatite/kaolinite nanocomposites for biomedical applications. Ceram Int. 2013;39(3):2757–2764.
[51] Bose S, Sarkar N, Banerjee D, Dudek A, Bandyopadhyay A. Calcium phosphate–ceramic systems in bone tissue

engineering: A review. Mater Today. 2018;21(10):659–675.